Journal of Quantitative Spectroscopy & Radiative Transfer 205 (2018) 127–134

Contents lists available at ScienceDirect

Journal of Quantitative Spectroscopy & Radiative Transfer

journal homepage: www.elsevier.com/locate/jqsrt

Retrieving the aerosol complex refractive index using PyMieScatt: A Mie computational package with visualization capabilities

Benjamin J. Sumlin[a], William R. Heinson[a], Rajan K. Chakrabarty[a,b,*]

[a] Center for Aerosol Science and Engineering Department of Energy, Environmental and Chemical Engineering, Washington University in St. Louis, MO 63130, USA

[b] McDonnell Center for the Space Sciences, Washington University in St. Louis, MO 63130, USA

ARTICLE INFO

Article history:
Received 20 July 2017
Revised 13 October 2017
Accepted 13 October 2017
Available online 16 October 2017

Keywords:
Aerosol optics
Mie theory
Python 3
Electromagnetic scattering and absorption
Open-source software

ABSTRACT

The complex refractive index $m = n + ik$ of a particle is an intrinsic property which cannot be directly measured; it must be inferred from its extrinsic properties such as the scattering and absorption cross-sections. Bohren and Huffman called this approach "describing the dragon from its tracks", since the inversion of Lorenz-Mie theory equations is intractable without the use of computers. This article describes *PyMieScatt*, an open-source module for Python that contains functionality for solving the inverse problem for complex m using extensive optical and physical properties as input, and calculating regions where valid solutions may exist within the error bounds of laboratory measurements. Additionally, the module has comprehensive capabilities for studying homogeneous and coated single spheres, as well as ensembles of homogeneous spheres with user-defined size distributions, making it a complete tool for studying the optical behavior of spherical particles.

1. Introduction

Bohren and Huffman's (B&H [1]) FORTRAN codes for Lorenz-Mie (Mie hereafter) theory [2] (BHMIE) have been the foundation and inspiration for generations of computer codes applicable to aerosol optics, written in many languages for a variety of problems. However, to our knowledge, a comprehensive collection of Mie codes is not available for Python, nor are there any open-source codes for solving the inverse Mie problem to retrieve the complex refractive index ($m = n + ik$) for a particle of known size parameter. Python (http://www.python.org) is an open-source scripting language that is popular for scientific, mathematical, and engineering computing. To address the lack of Mie optics software for Python, we wrote PyMieScatt, or the Python Mie Scattering package. PyMieScatt is a module, similar to a library in C. These codes are meant to be a tool for researchers, and can be used as either a standalone calculator or to develop custom Python scripts for specialized research or educational purposes.

PyMieScatt evolved from efforts to translate Christian Mätzler's collection of MATLAB scripts [3] into an open-source, platform-independent language and expand them for common problems found in experimental aerosol optics. Where Mätzler's work is a translation of the original BHMIE code, PyMieScatt has been written to emphasize readability and the mathematics of Mie Theory. Many additional components for computational work relevant to contemporary aerosol optics have been added. The package can:

i. calculate Mie efficiencies for extinction (Q_{ext}), scattering (Q_{sca}), absorption (Q_{abs}), radiation pressure (Q_{pr}), and backscatter (Q_{back}), as well as the asymmetry parameter (g) for a single particle in the Mie and Rayleigh regimes;
ii. as an extension of (i), calculate coefficients (β_{abs} and β_{sca}, for example) using measured, user-defined, or mathematically generated size distribution data for an ensemble of homogeneous particles;
iii. produce arrays for plotting the angular-dependent light scattering intensity for parallel and perpendicular polarizations in both θ-space and q-space [4] for a single particle or an ensemble of particles;
iv. calculate the four nonzero scattering matrix elements S_{11}, S_{12}, S_{33}, and S_{34} as functions of scattering angle;
v. do (i), (iii), and (iv) for coated spheres (core–shell particles);
vi. solve the inverse Mie problem for complex $m = n + ik$, given inputs of scattering, absorption, and size parameter for a single particle, or ensemble of particles given additional size distribution data and calculate solution regions bound by measurement uncertainty;
vii. as an extension of (vi), use additional measurements of backscatter efficiency (Q_{back}) or coefficient (β_{back}) to constrain the inverse problem to produce unique solutions.

* Correspondence author.
E-mail address: chakrabarty@wustl.edu (R.K. Chakrabarty).

https://doi.org/10.1016/j.jqsrt.2017.10.012
0022-4073/

Points (vi) and (vii) represent the major result of this work. While points (i) through (v) are useful for solving common problems, (vi) and (vii) use our development of a novel method for solving the inverse Mie problem for the complex refractive index when size parameter is known. Often, m is the unknown parameter in experiments involving a particle or a distribution of particles. Mie equations take m as an input, and so the problem of deriving it from measured data represents an inverse problem that is inconvenient to solve without the use of computers. Aerosol optics experiments frequently involve instruments designed to measure light scattering and absorption, such as photoacoustic spectrometers [5] and integrating nephelometers [6] which directly measure absorption and scattering coefficients β_{abs} and β_{sca}, respectively. Using Mie theory, one can calculate these parameters directly with knowledge of the analyte's size distribution and effective index of refraction (where it is known or assumed that the constituent particles are spherical). Conversely, with knowledge of optical behavior and morphology as measured by laboratory equipment, PyMieScatt can determine m by solving this inverse problem.

Simulation of scattering and absorption by an arbitrary particle is trivial with modern computing power and algorithms such as T-Matrix [7,8], finite-difference time-domain [9], the discrete dipole approximation [10], or a Mie theory implementation of choice. However, the inverse problem, whether it is constructed to solve for particle size, real m or complex m, is confounded by the multi-dimensional parameter space the equations require. Without a direct imaging technique like tomography, the problem must be constrained by measuring the particle morphology, making certain assumptions about the system, or careful parameterization of variables. There are numerous examples in the literature demonstrating the use of inversion techniques, in particular a variety of medical applications to infer properties about the health and morphology of blood cells [11–14], or to characterize the shape of individual bacteria [15–17]. Previous work to invert optical measurements to reconstruct particle properties are often constrained to the particle size and real m [18,19], or use measurements at multiple angles to determine m [11].

We constrain the inverse problem by measuring or assuming the size of a spherical, homogeneous particle (or size distribution of an ensemble thereof), and knowing the wavelength of light illuminating it. Our parameter space is therefore less complex and our method constructs an inverse problem using measurements of scattering and absorption, which can be further constrained by introducing backscattering efficiency, a third independent parameter.

2. The inverse Mie problem

PyMieScatt uses a highly visual, geometric method to invert the Mie problem and calculate m for a single particle (given Q_{abs}, Q_{sca}, the wavelength, and diameter) or for an ensemble of particles (given β_{abs}, β_{sca}, the wavelength, and a size distribution). This contour intersection method visualizes various optical parameter spaces as functions of n and k and looks for intersections in the curves defined by optical measurements. Additionally, we include a strictly numerical approach that borrows certain principles from the visual technique and minimizes errors in the retrieval by brute-force iterative methods.

2.1. The contour intersection approach

The contour intersection inversion method determines the index of refraction by first computing $Q_{sca}(n,k)$ and $Q_{abs}(n,k)$ for a given wavelength and particle diameter across a range of n and k, then identifying the contours corresponding to measured Q_{sca} and Q_{abs}, and finally identifying their intersections in n-k space. Intersections represent values of m that would produce the desired Q_{sca} and Q_{abs}. Similarly, this method can also find the effective m of a size distribution of spherical particles by computing $\beta_{sca}(n,k)$ and $\beta_{abs}(n,k)$ and following the same procedure.

Fig. 1 illustrates the theory of this process with an example. With ideal laboratory equipment, assume a test particle whose diameter was measured to be 300 nm, and its 375 nm Q_{sca} and Q_{abs} were 1.315 and 1.544, respectively. First, calculate the Q_{sca} and Q_{abs} surfaces over a range of n and k (panel A, note that we have added contour lines to the surfaces and have plotted k on a logarithmic scale to reveal the complex surface geometry). Then, we identify the contours corresponding to $Q_{sca} = 1.315$ and $Q_{abs} = 1.544$ (panel B). Finally, we project those contours to n-k space and locate their intersections (panel C, where k is plotted on a linear scale).

Once solutions are found, forward Mie calculations are performed, the results are compared to the input values, and their relative errors, which we denote Err(Q), are computed as

$$\mathrm{Err}(Q_{candidate}) = 100\% \times \left| \frac{Q_{candidate} - Q_{input}}{Q_{input}} \right| \quad (1)$$

Solutions are displayed on the output graph along with the relative errors in both scattering and absorption.

2.2. Constraining the inverse problem

In Section 2.1, when only Q_{sca} and Q_{abs} are specified, we see that multiple valid solutions of the inversion may exist. Any consideration of the inverse problem would be incomplete without attempting to seek all solutions and evaluate them for physical meaning. For many laboratory experiments, this may be the only practical approach. However, if an additional measured parameter independent of Q_{sca} and Q_{abs} is available, then the solution may be constrained. A favorable choice is to measure the backscatter efficiency Q_{back} with a capable nephelometer (e.g., the TSI Integrating Nephelometer 3563 or Ecotech Aurora 3000). Our example particle from the previous section was found to have $Q_{back} = 0.201$. We calculate the Q_{back} surface and project the desired contour onto the n-k plane (Fig. 2A, with Q_{back} truncated above 3.0) and plot all three parameters together to find a unique intersection of the contours at $m = 1.77 + 0.63i$, shown in Fig. 2B. In PyMieScatt, this constraint technique is automatically applied when the user specifies Q_{back} in the function call.

In laboratory studies, it is unlikely that instruments will measure particle properties so perfectly, and when considering errors associated with aerosol light scattering and absorption measurements (which are commonly given as a mean and standard deviation over a given averaging time), the refractive index will have associated error as well. Therefore, the solution in n-k space is best represented as a region rather than a point. The visualization of these error regions is discussed in Section 4.

2.3. The survey-iteration method

About 20–50% of the computing overhead for the contour intersection method is devoted to the plotting library. If a non-visual approach is needed by a user (i.e., to include a retrieval of m in existing programs), a faster, strictly numerical version of the contour intersection algorithm is included in PyMieScatt, which we call the survey-iteration method. We present an overview of the method here, and complete details may be found in the SM.

This inversion method is a brute-force, error-minimization technique. Inversion by iteration is a downhill-only algorithm that gravitates toward the solution nearest its initial guess, and it seeks local minimum values of error per Eq. (1). This approach estimates the number of solutions for a non-unique problem by first doing a coarse, rapid survey of the scattering and absorption parameter spaces, which is essentially a restrained, low-resolution non-geometric version of the contour intersection method.

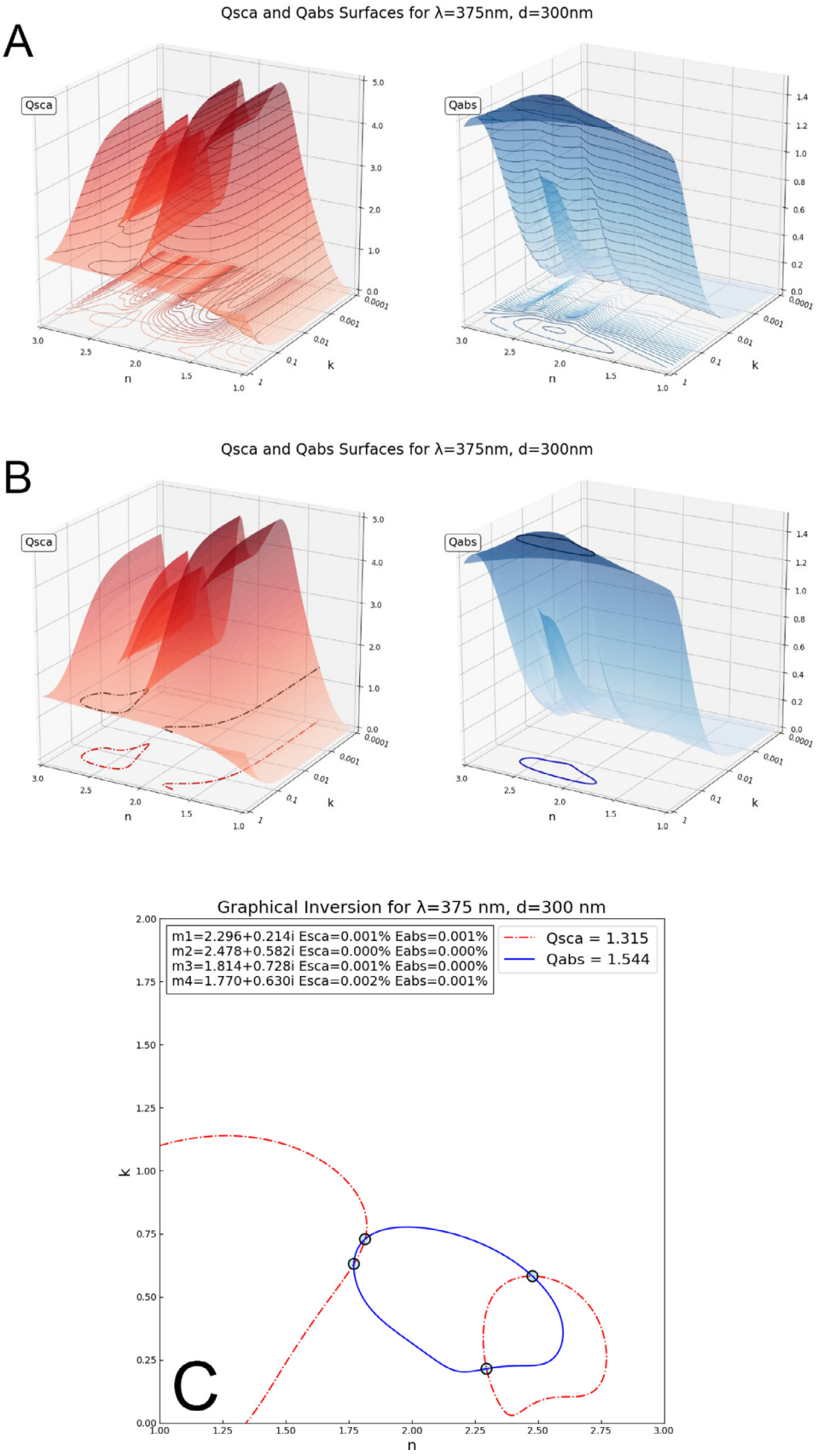

Fig. 1. (A) The Q_{sca} (left, red) and Q_{abs} (right, blue) surfaces for a range of m with $\lambda = 375$ nm and $d = 300$ nm. (B) The contours where $Q_{sca} = 1.315$ and $Q_{abs} = 1.544$. (C) The contours projected to n-k space and their intersections identified. (For interpretation of the references to color in this figure legend, the reader is referred to the web version of this article.)

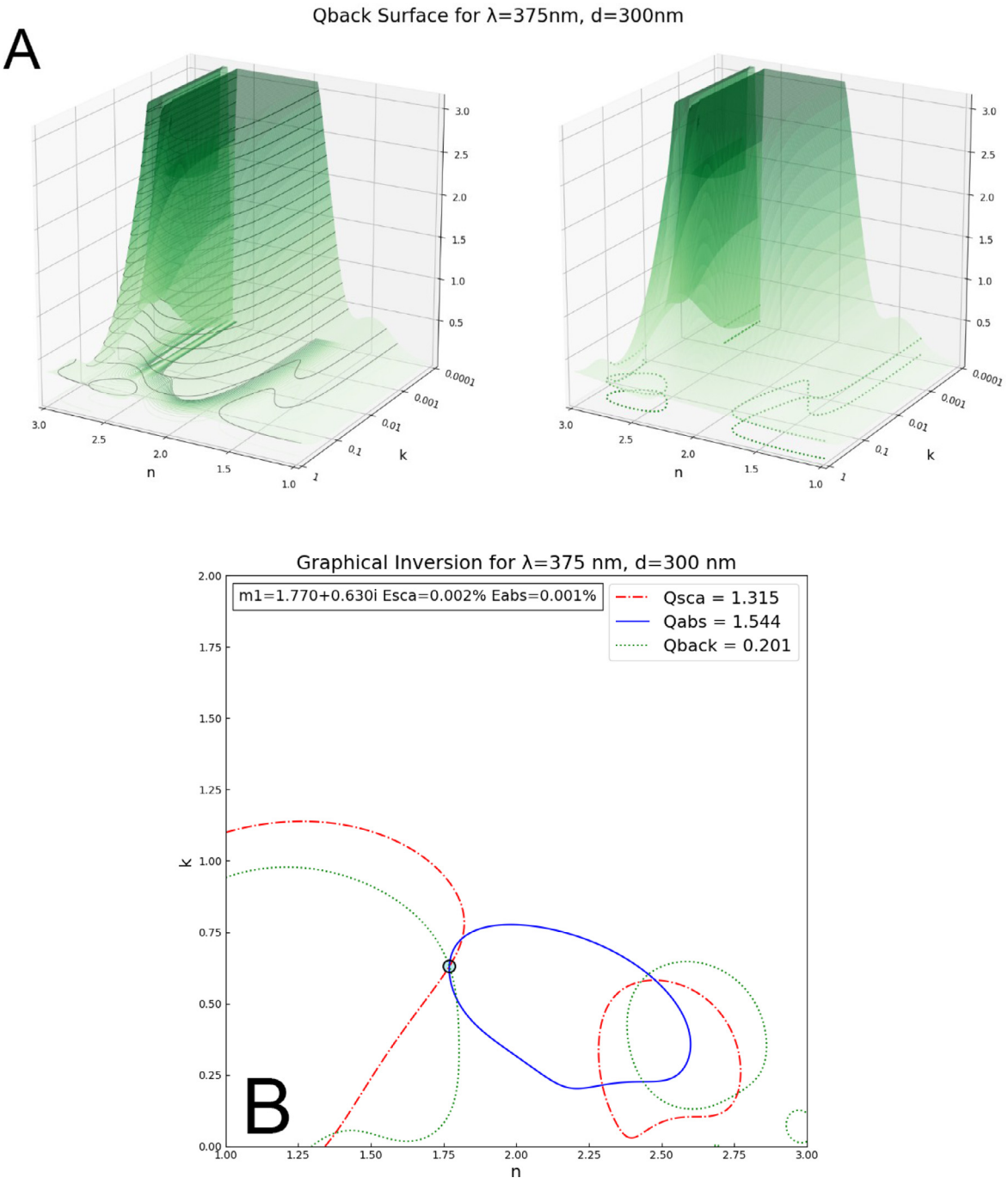

Fig. 2. (A) The Q_{back} surface for a range of m with $\lambda = 375$ nm and $d = 300$ nm (left), and the contours where $Q_{back} = 0.201$ (right). (B) Q_{sca}, Q_{abs}, and Q_{back} contours projected to n-k space and their unique intersection identified at $m = 1.77 + 0.63i$. E_{sca} and E_{abs} follow from Eq. (1) and denote the absolute errors in the Q_{sca} and Q_{abs} values produced by forward calculations using the retrieved refractive index versus the input values of Q_{sca} and Q_{abs}.

From this, the number of distinct solutions is estimated and an initial guess of m is generated for each intersection. The algorithm begins at an initial guess and iterates through n-k space using small changes of n and k separately, calculating Q_{sca} and Q_{abs} at each step. The calculated efficiencies are compared to the input values, and Eq. (1) computes $\mathrm{Err}(Q_{i,s})$, where $Q_{i,s}$ is the calculated efficiency (either scattering or absorption) at step s. As error decreases, step sizes Δn and Δk change depending on the magnitude of the relative error. When the calculations are close to the correct value, step s will overshoot, error will increase, and the difference

$$\mathrm{Err}(Q_{i,s-1}) - \mathrm{Err}(Q_{i,s}) \tag{2}$$

becomes negative. When this happens, the routine changes direction (by multiplying either Δn or Δk by -1), and continues stepping. Once four such sign changes occur, the routine reduces the step size and continues searching. Since Q_{sca} and Q_{abs} are both dependent on n and k, the algorithm alternates between varying n and k several times, with the final iteration using the smallest specified step sizes. This process is repeated for each initial guess determined from the survey, and the output from each is the derived m as well as the associated errors per Eq. (1). This method is faster than the contour intersection method, though its primary drawback is the handling of the errors associated with the input values. Since the survey-iteration method is strictly numerical, it

Table 1
Examples of solutions found and time required by each algorithm when analyzing a random system.

Method \ Results		Solutions found	Run time (s)
Single particle	Contour intersection	5	2.343
	Survey-iteration	5	1.485
Size distribution	Contour intersection	1	81.660
	Survey-iteration	1	38.316

cannot accurately predict the geometry of the allowed solution region discussed in Section 4.

2.4. Comparisons and timing

We performed calculations on randomly-generated systems of wavelength and particle size using the contour intersection method and the survey-iteration method to compare timing and robustness. Table 1, while not an exhaustive comparison, shows two examples and illustrates the difference in computing overhead required.

3. Applications

3.1. Refractive index of atmospheric aerosols and handling of measurement errors

Recently, a study conducted at the authors' laboratory investigated the effects of photooxidation on the absorption properties of light absorbing organic aerosol, or brown carbon (BrC) [20]. A pre-release version of PyMieScatt was used to determine the effective refractive indices of BrC particles using β_{sca} and β_{abs} measurements from integrated photoacoustic-nephelometer spectrometers at 375, 405, and 532 nm, and size distribution measurements from an SMPS. Electron microscopy revealed their morphology to be spherical and homogeneous. Determination of m partially motivated the development of PyMieScatt.

Fig. 3 follows the same procedure from Section 2.1. In panel A, we show the β_{sca} and β_{abs} surfaces. In panel B, we locate the contours of 375 nm scattering and absorption measurements of $\beta_{sca} = 5087.2 \pm 361.7$ Mm^{-1} and $\beta_{abs} = 858.3 \pm 46.0$ Mm^{-1}, and project those contours to the n-k plane. In panel C, we locate their intersection and find the effective $m = 1.576 + 0.029i$. As mentioned in Section 2.2, laboratory measurements have an associated uncertainty. This is often reported as the standard deviation of a time-averaged signal, or in the case of physical measurement, the degree of spread in a transfer function. This uncertainty propagates to the retrieval of m. PyMieScatt assumes the physical measurements are accurate and treats errors in optical measurements by visually identifying regions of allowed m as patches of red (indicating the error associated with scattering) and blue (absorption). Where the regions overlap are areas of allowed m, where valid solutions within measurement error may exist. This is the strength of the visual method, since not only can we see where solutions may be found, we can also see where they may not.

We have shown in Section 2.1 that it is possible for Mie theory inversions to have multiple solutions when only two inputs are given, and it is reasonable to ask whether inversions in laboratory studies are yielding the "correct" solution. Here, we show that a distribution of aerosol is likely to have a single physically valid solution, without the need for an additional measured parameter. For atmospheric aerosol, n and k have been observed in the range of 1.3 to 2.0 and 10^{-9} to 1.0, respectively [21]. For the sake of illustration, we will extend the analysis of the previous example and evaluate n in the range of 1.0 to 20 while constraining k to between 10^{-3} and 1.0. The result is given in Fig. 4. The measurement error regions begin to overlap around $n = 5$ and major contours intersect several times at $m = 8.417 + 0.027i$, $8.840 + 0.025i$, $8.941 + 0.026i$, $9.592 + 0.027i$, and $9.897 + 0.027i$. However, only the solution at $m = 1.576 + 0.029i$ can be considered valid based on our knowledge of the particles in question. This solution is not unique in the mathematical sense, but is the only one that is consistent with physical intuition. We therefore see that β_{back} may not be required to obtain a valid, constrained calculation of m for a polydisperse ensemble of particles.

3.2. The vanishing degenerate solutions

We have demonstrated that with measurements of only Q_{abs} and Q_{sca}, the inverse Mie problem for single particles may have multiple solutions, while for a size distribution and measurements of β_{abs} and β_{sca}, the realistic solution is likely unique (within reason for atmospheric aerosol). Extraneous solutions vanish when we move from a single particle to an ensemble. It is natural to wonder what mechanism governs this transition. PyMieScatt's visualization capabilities were used to study this phenomenon.

Consider a δ-distribution of 10^6 particles cm^{-3}, each 300 nm in diameter, with $m = 1.60 + 0.36i$. This δ-distribution can be considered the limiting case of a lognormal distribution with $d_{pg} = 300$ and $\sigma_g = 1$. As σ_g increases from 1.0 to 2.0, the distribution behaves like a typical ensemble of aerosols. We plotted the β_{sca} and β_{abs} surfaces at several values of increasing σ_g, along with the particle size distribution and the solution for m in n-k space produced by the contour intersection inversion method. We note that the shape of the β_{abs} surface remains mostly constant throughout, while the β_{sca} surface undergoes the most change. We see the local minimum around $m = 2.60 + 0.40i$ lift and flatten as σ_g increases. By $\sigma_g \approx 1.177$, the global minimum responsible for the extra solutions has already been lifted above the measurement contours. In this case, it is the scattering behavior of the system that dictates the transition to a unique solution. Other systems may behave similarly.

We have prepared an animation of this phenomenon which can be found in the online supplement to this article. Fig. 5 shows several frames of this animation giving an overview of how extra solutions vanish and the desired solution remains unchanged.

4. Concluding remarks

We conclude by briefly comparing PyMieScatt to other Python implementations of Mie theory. Mie theory has previously been implemented in Python, but not to the level of sophistication of our libraries. Table 2 summarizes the features of several Mie codes available online. In addition to the Mie inversions, PyMieScatt contains over twenty functions for Mie efficiencies of homogeneous particles and core–shell particles; wavelength, diameter, and size parameter ranges; angular scattering functions for single or size distributions of homogeneous particles, as well as single core–shell particles; and functions for arbitrary size distributions, including mathematically-generated k-modal lognormal distributions.

PyMieScatt has been applied successfully to theoretical and experimental problems. Our contour intersection inversion method provides visual insight to the problem and aids in identifying multiple solutions and evaluating them for physical validity. Using this method, we have shown how inversions on polydisperse size distributions are unlikely to encounter the issue of multiple solutions. PyMieScatt's code base is open-source, documented, and actively maintained. It was originally developed to aid in very specific calculations to improve analysis of carbonaceous aerosol optical properties, but has evolved to be a general and comprehensive set of tools.

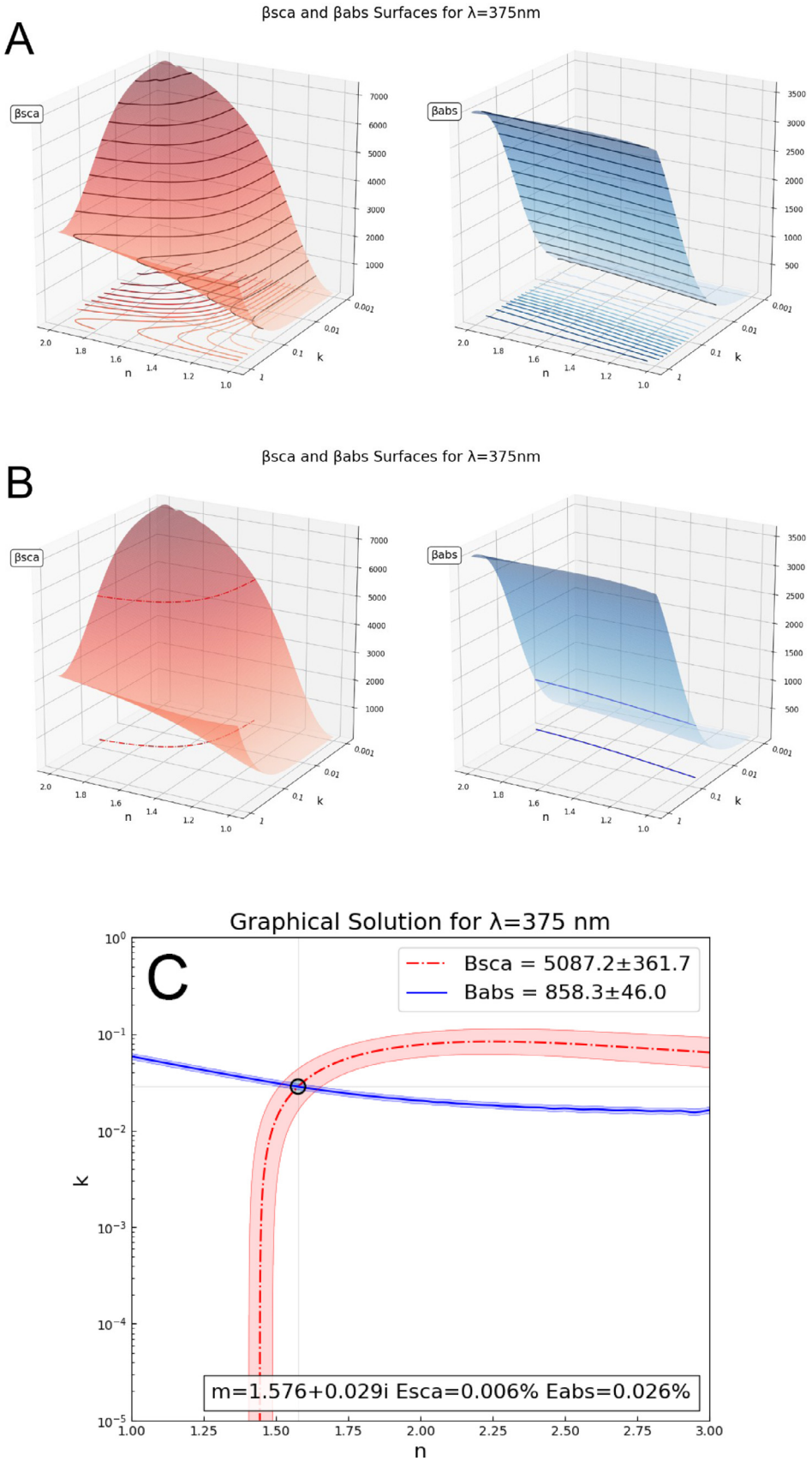

Fig. 3. (A) The β_{sca} (left, red) and β_{abs} (right, blue) surfaces for a range of m for a size distribution illuminated at $\lambda = 375$ nm. (B) The contours of measured $\beta_{sca} = 5087.2 \pm 631.7$ Mm^{-1} and $\beta_{abs} = 858.3 \pm 46.0$ Mm^{-1}. (C) The contours projected to n-k space and their intersection identified at $m = 1.576 + 0.029i$. The shaded regions denote the errors associated with measurements. The overlapping red and blue regions indicate where a valid solution within measurement error may exist. E_{sca} and E_{abs} follow from Eq. (1) and denote the absolute errors in the β_{sca} and β_{abs} values produced by forward calculations using the retrieved refractive index versus the input values of β_{sca} and β_{abs}. (For interpretation of the references to color in this figure legend, the reader is referred to the web version of this article.).

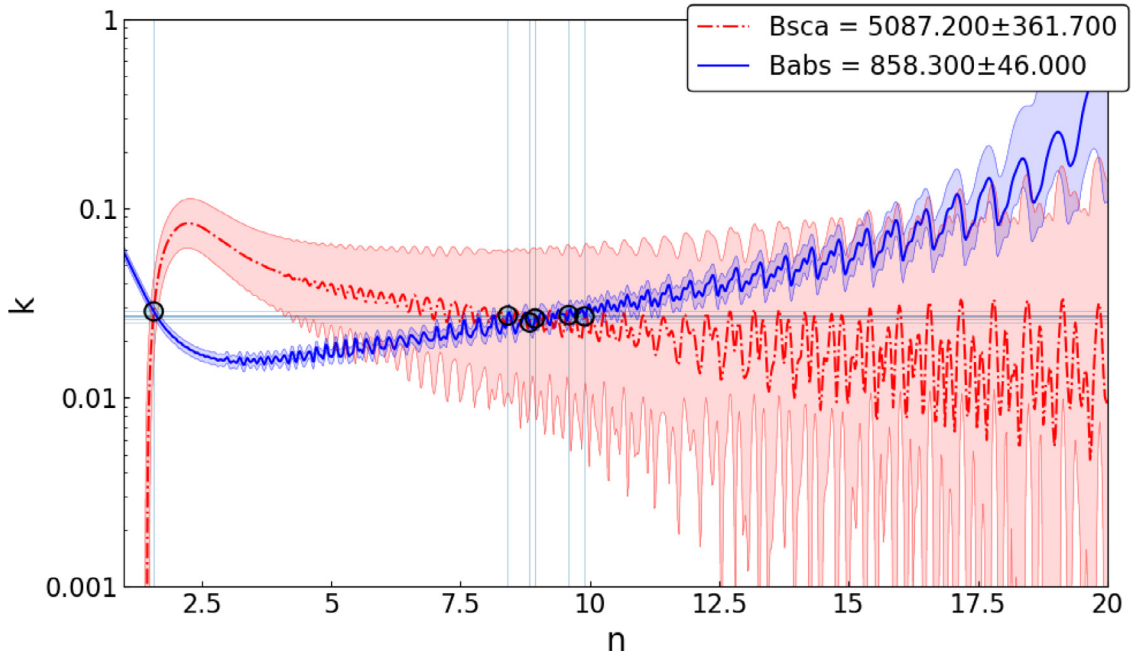

Fig. 4. The contour intersection inversion method applied to an extended range of n from 1.0 to 20.0. The valid solution occurs at $m = 1.576 + 0.023i$ as before, though several extraneous solutions appear between $n = 8$ and 10. The shaded regions denote the errors associated with measurements, and we have removed some annotations for clarity.

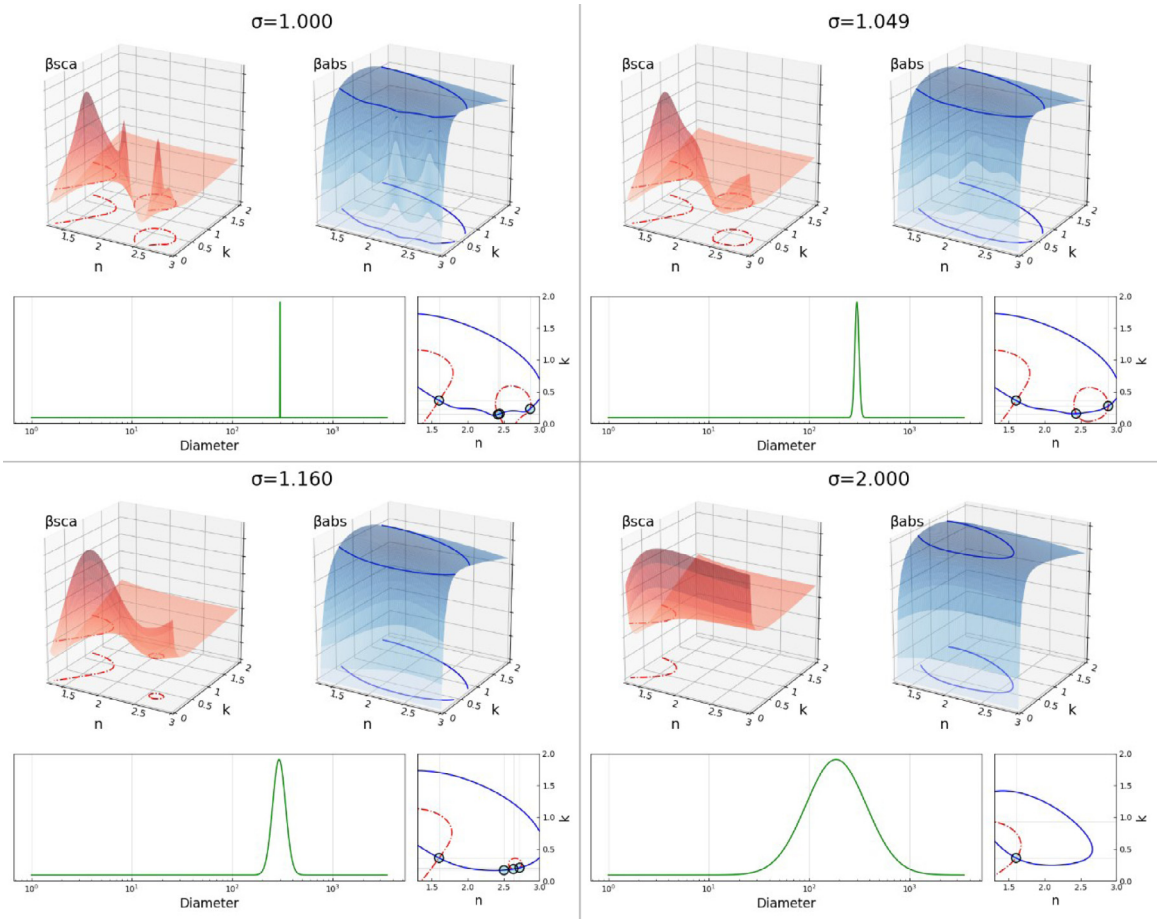

Fig. 5. The effects on the β_{abs} (blue) and β_{sca} (red) contours in n-k space as σ_g increases. (For interpretation of the references to color in this figure legend, the reader is referred to the web version of this article.).

Table 2
Features of Python Mie codes found online.

Feature \ Package	Py-Mie	Pymiecoated	bhMie.Py	**PyMieScatt**
Homogeneous Sphere	√[a]	√[b]	√[a]	√[c]
Coated sphere	√[a]	√[b]		√[c]
Lognormal distribution	unimodal			k-modal
Arbitrary distribution				√
Parameter ranges				√
Angular functions		√[d]	√[e]	√[f]
Single-particle inversion				√
Distribution inversion				√
Documentation	limited			full
Examples		one		several
Active maintenance				√

[a] scattering, absorption, and asymmetry parameter.
[b] scattering, absorption, and backscatter efficiencies; asymmetry parameter; backscatter ratio.
[c] extinction, scattering, absorption, and backscatter efficiencies; asymmetry parameter; backscatter ratio; radiation pressure.
[d] only S_1 and S_2 scalars as functions of a single scattering angle.
[e] S_1 and S_2 arrays over range of all scattering angles.
[f] S_1 and S_2 arrays over range of all or user-defined scattering angles; scattering intensity functions for polarized and unpolarized light.

Data availability

Source code for PyMieScatt is available at https://github.com/bsumlin/PyMieScatt. Details on the experimental setup used for the example in Section 3.1 are available in Ref. [20], and the raw data is available from the authors upon request.

Funding

This work was supported by the NSF under Grant Nos. AGS-1455215 and CBET-1511964, and NASA ROSES under Grant No. NNX15AI66G.

Supplementary materials

Supplementary material associated with this article can be found, in the online version, at doi:10.1016/j.jqsrt.2017.10.012.

References

[1] Bohren CF, Huffman DR. Absorption and scattering of light by small particles. John Wiley & Sons, Inc.; 1983.
[2] Mie G. Beiträge zur Optik trüber Medien, speziell kolloidaler Metallösungen. Ann Phys 1908;330:377–445.
[3] Mätzler C. MATLAB functions for Mie scattering and absorption. University of Bern: Institute of Applied Physics; 2002.
[4] Sorensen CM. Q-space analysis of scattering by particles: A review. J Quant Spectrosc Radiat Transfer 2013;131:3–12.
[5] Arnott WP, Moosmüller H, Fred Rogers C, Jin T, Bruch R. Photoacoustic spectrometer for measuring light absorption by aerosol: instrument description. Atmos Environ 1999;33:2845–52.
[6] Abu-Rahmah A, Arnott WP, Moosmüller H. Integrating nephelometer with a low truncation angle and an extended calibration scheme. Meas Sci Technol 2006;17:1723–32.
[7] Mishchenko MI, Travis LD, Mackowski DW. T-matrix computations of light scattering by nonspherical particles: a review. J Quant Spectrosc Radiat Transfer 1996;55:535–75.
[8] Mackowski DW, Mishchenko MI. Calculation of the T matrix and the scattering matrix for ensembles of spheres. JOSA A 1996;13:2266–78.
[9] Yang P, Liou KN. Finite difference time domain method for light scattering by nonspherical and inhomogeneous particles. In: Light scattering by nonspherical particles. Elsevier; 2000. p. 173–221.
[10] Yurkin MA, Hoekstra AG. The discrete dipole approximation: an overview and recent developments. J Quant Spectrosc Radiat Transfer 2007;106:558–89.
[11] Tycko DH, Metz MH, Epstein EA, Grinbaum A. Flow-cytometric light scattering measurement of red blood cell volume and hemoglobin concentration. Appl Opt 1985;24:1355.
[12] Moskalensky AE, Yurkin MA, Konokhova AI, Strokotov DI, Nekrasov VM, Chernyshev AV, et al. Accurate measurement of volume and shape of resting and activated blood platelets from light scattering. J Biomed Opt 2013;18:017001.
[13] Kim Y, Shim H, Kim K, Park H, Jang S, Park Y. Profiling individual human red blood cells using common-path diffraction optical tomography. Sci Rep-Uk 2014;4.
[14] Caramanica F. A method based on particle swarm optimization to retrieve the shape of red blood cells: a preliminary assessment. Prog Electromagn Res M 2012;27:109–17.
[15] Wyatt PJ. Cell wall thickness, size distribution, refractive index ratio and dry weight content of living bacteria (*Stapylococcus aureus*). Nature 1970;226:277–9.
[16] Wyatt PJ, Phillips DT. Structure of single bacteria from light scattering. J Theoret Biol 1972;37:493–501.
[17] Konokhova AI, Gelash AA, Yurkin MA, Chernyshev AV, Maltsev VP. High-precision characterization of individualE. colicell morphology by scanning flow cytometry. Cytom Part A. 2013;83A:568–75.
[18] Maltsev VP, Lopatin VN. Parametric solution of the inverse light-scattering problem for individual spherical particles. Appl Opt 1997;36:6102.
[19] Romanov AV, Konokhova AI, Yastrebova ES, Gilev KV, Strokotov DI, Chernyshev AV, et al. Spectral solution of the inverse Mie problem. J Quant Spectrosc Radiat Transfer 2017;200:280–94.
[20] Sumlin BJ, Pandey A, Walker MJ, Pattison RS, Williams BJ, Chakrabarty RK. Atmospheric photooxidation diminishes light absorption by primary brown carbon aerosol from biomass burning. Environ Sci Tech Lett 2017, doi:10.1021/acs.estlett.7b00393.
[21] Levoni C, Cervino M, Guzzi R, Torricella F. Atmospheric aerosol optical properties: a database of radiative characteristics for different components and classes. Appl Opt 1997;36:8031.